NANOSYSTEMS:
PHYSICS, CHEMISTRY, MATHEMATICS

Original article

Korotkova N.A., et al. *Nanosystems: Phys. Chem. Math.*, 2024, **15** (6), 855–866.
http://nanojournal.ifmo.ru
**DOI 10.17586/2220-8054-2024-15-6-855-866**

# Development of spectral methods for the analysis of nanocized ferrogarnets of the $Y_{3-x}Ce_xFe_{5-y}Ga_yO_{12}$ composition

Natalia A. Korotkova[1,a], Alexandra A. Arkhipenko[1,b], Maria N. Smirnova[1,c], Vasilisa B. Baranovskaya[1,d], Marina S. Doronina[1,e], Valerii A. Ketsko[1,f], Galina E. Marina[1,g]

[1]Kurnakov Institute of General and Inorganic Chemistry of the Russian Academy of Sciences, Moscow, Russia

[a]natalya.korotkova.95@mail.ru, [b]alexandra622@mail.ru, [c]smirnovamn@igic.ras.ru, [d]baranovskaya@list.ru, [e]ms.semenova@gmail.com, [f]ketsko@igic.ras.ru, [g]gelim@mail.ru

Corresponding author: N. A. Korotkova, natalya.korotkova.95@mail.ru

PACS 81.07.Wx, 62.20.Qp, 78.20.-e

ABSTRACT The study and development of yttrium-iron garnets are in demand and promising when creating materials for integrated optics and magnetic microelectronics. The authors synthesized nanosized cerium-substituted yttrium-iron-gallium garnet of the composition $Y_{3-x}Ce_xFe_{5-y}Ga_yO_{12}$ (where x = 0.4 – 0.5, and y = 2.4 – 2.6), which is characterized by improved magnetic and optical properties. However, the efficiency of applying this material directly depends on the chemical purity of the source materials, as well as the elemental composition of the intermediate and final products. In this regard, the development of multi-element, selective and accurate methods of analysis is an urgent task. As a result of the studies, methods for spectral analysis of cerium-substituted yttrium-iron-gallium garnet were developed. The conditions for determining target analytes (Mg, Al, Si, Ca, Sc, Cr, Mn, Fe, Co, Ni, Cu, Zn, Ga, Se, Y, Cd, Sn, Te, La, Ce, Pr, Nd, Sm, Eu, Gd, Tb, Dy, Ho, Er, Tm, Yb, Lu, Pb) in the materials in question were studied and established using X-ray fluorescence spectrometry (XRF), arc atomic emission spectrometry (AAES) and inductively coupled plasma mass spectrometry (ICP-MS). Approaches to reducing and eliminating the main spectral and non-spectral interferences in the methods studied were proposed. A comprehensive complementary approach to the analytical control of garnets of the $Y_{3-x}Ce_xFe_{5-y}Ga_yO_{12}$ composition was developed, which ensures high accuracy and reliability of the results, and allows one to expand the nomenclature of target analytes and the boundaries of the determined contents.

KEYWORDS yttrium-iron-gallium garnet, X-ray fluorescence spectrometry, arc atomic emission spectrometry, inductively coupled plasma mass spectrometry, analysis.

ACKNOWLEDGEMENTS This research was performed using the equipment of the JRC PMR IGIC RAS and JRC of GIREDMET. This work was supported by the Ministry of Science and Higher Education of the Russian Federation as part of the State Assignment of the Kurnakov Institute of General and Inorganic Chemistry of the Russian Academy of Sciences.

FOR CITATION Korotkova N.A., Arkhipenko A.A., Smirnova M.N., Baranovskaya V.B., Doronina M.S., Ketsko V.A., Marina G.E. Development of spectral methods for the analysis of nanocized ferrogarnets of the $Y_{3-x}Ce_xFe_{5-y}Ga_yO_{12}$ composition. *Nanosystems: Phys. Chem. Math.*, 2024, **15** (6), 855–866.

## 1. Introduction

One of the promising and rapidly developing directions in modern materials science is the development of functional materials for integrated optics and magnetic microelectronics. Ferrogarnets have been progressed among the materials with the necessary magnetic and optical properties [1]. Cerium containing yttrium ferrogranates have the best characteristics in terms of the combination of optical, magneto-optical activity and magneto-optical quality factor [1–6].

However, due to the large ionic radius of $Ce^{3+}$ (1.14 Å) ferrogarnet of the hypothetical elemental composition – $Ce_3Fe_5O_{12}$ does not exist in the form of ceramics and single crystals [7, 8]. Because of this fact, the possibility of obtaining single-phase cerium-substituted ferrogarnets with the maximum possible $Ce^{3+}$ content is of particular relevance, for example, by replacing part of the $Y^{3+}$ ions in $Y_3Fe_5O_{12}$ with $Ce^{3+}$ [7–11]. Such materials were obtained in a number of studies [12–14]. At the same time, the $Ce^{3+}$ content in garnet in these studies, according to X-ray diffraction (XRD), did not reach 8 wt. %, for example, $Ce_{0.122}Y_{2.878}Fe_5O_{12}$ [12–14].

The authors previously obtained a single-phase ferrogarnet with an increased Ce content – $Y_{2.5}Ce_{0.5}Fe_{2.5}Ga_{2.5}O_{12}$ [7]. The $Ce^{3+}$ content in the material was increased by annealing $Y_{2.5}Ce_{0.5}Fe_{2.5}Ga_{2.5}O_{12}$ in a vacuum and replacing some of the $Fe^{3+}$ ions with $Ga^{3+}$. The introduction of $Ga^{3+}$ ions into the composition together with $Ce^{3+}$ enabled to compensate for structural limitations and contributed to the stabilization of $Y_{2.5}Ce_{0.5}Fe_{2.5}Ga_{2.5}O_{12}$ [7].

It is noteworthy that while developing materials for integrated optics, the presence of impurity elements (Mg, Al, Si, Ca, Sc, Cr, Mn, Co, Ni, Cu, Zn, Se, Cd, Sn, Te, La, Pr, Nd, Sm, Eu, Gd, Tb, Dy, Ho, Er, Tm, Yb, Lu, Pb) and a disturbance of the matrix and alloying component ratio (Fe, Ga, Y, Ce) can lead to a decrease in the magnetic and optical properties of the final product [15–19]. In this regard, analytical control of ferrogarnets is necessary at all stages of its production. Spectral methods, namely X-ray fluorescence (XRF), arc atomic emission (AAES) and inductively coupled plasma mass spectrometry (ICP-MS), are promising for solving this task. The analytical methods listed have high accuracy, sensitivity and versatility [20–34]. XRF has a wide range of detectable concentrations and is prospective to express control of the matrix and alloying component ratio in the process of developing and producing complex materials [23–26]. The advantages of AAES method are the possibility of simultaneous determination of a large number of elements, high sensitivity and the absence of the need to dissolve the sample [20–22]. ICP-MS is one of the most widely used methods to determine low levels of trace elements in sample solutions. The advantages of ICP-MS include high sensitivity, a wide range of contents being determined, the possibility of using universal standard solutions to construct a calibration curve and verify the result accuracy [27–34]. Accordingly, the use of XRF, AAES and ICP-MS methods is promising for allowing for the control of the target composition of complex materials, including cerium-substituted yttrium-iron-gallium garnet.

However, the presented methods (XRF, AAES, ICP-MS) have a number of limitations. Namely, spectral and non-spectral interference of various types [20–34]. The overlapping of analyte signals is primarily highlighted. This problem is especially acute when analyzing materials containing rare earth elements (REE) as the main ones. This problem is solved by conducting a set of studies aimed at a detailed study of the obtained spectra and the influence of the analysis conditions on the intensity and stability of the signal of the analytes determined, and searching for an approach to considering the background signal and constructing a calibration dependence [20–34].

This article is devoted to the development of approaches to reducing and eliminating various types of interference in XRF, AAES and ICP-MS analysis of nanosized ferrogarnets of the composition $Y_{3-x}Ce_xFe_{5-y}Ga_yO_{12}$ ($x$ = 0.4–0.5, $y$ = 2.4–2.6).

## 2. Experimental part

### 2.1. Materials

Synthesis of $Y_{3-x}Ce_xFe_{5-y}Ga_yO_{12}$($x$ = 0.4–0.5, $y$ = 2.4–2.6) was carried out by gel combustion [7]. For this purpose, stoichiometric amounts of high-purity yttrium carbonate ($Y_2(CO_3)_3{\cdot}3H_2O$), cerium nitrate ($Ce(NO_3)_3$), carbonyl iron (Fe) and metallic gallium (Ga) were dissolved in dilute nitric acid ($HNO_3$ – 70 %). Then polyvinyl alcohol $[–CH_2CH(OH)–]_n$ (PVA) was added to the resulting solution, based on the calculation of 0.12 mol PVA per 0.01 mol ferrite, as well as ammonium nitrate ($NH_4NO_3$) in the amount of 0.12 mol per 0.01 mol ferrite. The reaction mixtures were evaporated in a reactor at 90°C with constant stirring until they became gels.

As the temperature increased above 100°C, the gels burnt into finely dispersed yellow-beige powders. After cooling, the powders were dispersed using a ball mill and annealed at 750°C in a furnace for 5 hours at a pressure of $\approx 1{\cdot}10^{-2}$ Pa. This mode of heat treatment was due to the need to exclude the possibility of $Ce^{3+}$ cation oxidation.

### 2.2. Methods

X-ray diffraction was performed using a Bruker D8 Advance diffractometer (BrukerOptik Gmb H, Germany). The following operating parameters were used to obtain the results: a radiation – CuK$\alpha$, an angle range $2\theta$ = 10°–70°, a scanning step – 0.0133° and a counting time of 0.3 sec per step.

The morphology of the powders was performed using scanning electron microscopy (SEM) on a TESCAN AMBER GMH device (Tescan, Czech Republic).

To primarily determine the ratio of the matrix and alloying components in the material, XRF analysis method was used. A wavelength-dispersive X-ray fluorescence spectrometer SPECTROSCAN MAX GVM (Spectron Ltd., St. Petersburg, Russian Federation) was performed (Table 1). Quantitative determination was carried out using the fundamental parameters method (FPM).

TABLE 1. Instrumental operating conditions of the X-ray fluorescence spectrometer

| Element | Analytical Line | Wavelength, nm | Crystal analyzer | Reflection Order | Exposure Time, sec | Tube Current, mÅ |
|---|---|---|---|---|---|---|
| Fe | K$\beta$ | 0.1757 | LiF200 | 1 | 10 | 0.5 |
| Ga | K$\beta$ | 0.1208 | LiF200 | 1 | 10 | 0.5 |
| Y | K$\alpha$ | 0.0830 | LiF200 | 1 | 10 | 0.1 |
| Ce | L$\alpha$ | 0.2561 | LiF200 | 1 | 10 | 1.5 |

Arc atomic emission spectrometry and inductively coupled plasma mass spectrometry were performed to determine target impurity elements.

The studies into the analysis conditions of arc atomic emission method were carried out on a high-resolution spectrometer Grand-Globula (VMK-Optoelectronics, Russian Federation) (Table 2).

TABLE 2. Instrumental operating conditions of the arc atomic emission spectrometer

| Current type | Direct |
|---|---|
| Current strength,Å | 15 |
| Configuration of the lower graphite electrode | Electrode with a neck below the bottom of the crater (“glass”) |
| The thickness of the walls of the lower electrode is not more than, mm | 1 |
| Configuration of the upper graphite electrode | Cone 60° |
| Mass ratio of the sample to the graphite powder | 5:1 |
| Carrier | NaCl |
| Distance between the upper and lower electrodes, mm | 3 |
| Exposure time, sec | 60 |
| Analytical lines of elements being determined, nm | Mg 277.98, 285.21; Al 266.04, 309.27; Si 288.16, 243.52; Ca 317.93; Cr 284.98, 301.49; Mn 279.48; Co 242.49, 340.92; Ni 225.38; 305.08; Cu 240.67; Zn 213.86; Se 206.28; Cd 226.50; Sn 224.61, 242.17; Te 214.28, 238.58; La 338.09; Pr 316.37; Nd 430.36; Sm 442.43; Eu 281.39; Cd 301.01; Tb 332.44; Dy 317.00, 340.78; Ho 311.85, 345.60; Er 339.20; Tm 313.13; Yb 328.94; Lu 261.54, 291.14; Pb 244.62, 261.42 |

ICP-MS analysis conditions were studied using a NexION® 1000 spectrometer (PerkinElmer, USA) (Table 3).

Inductively coupled plasma optical-emission spectrometry (ICP-OES) was used as a control method. Earlier we studied and selected the conditions for analyzing the material under examination using ICP-OES method [35].

### 2.3. Sample preparation

Before conducting XRF analysis, the sample was pressed on a boric acid substrate using a PLG-12 laboratory hydraulic press (LabTools, Russian Federation). The pressure did not exceed 100 bar. The mass of the nanocrystalline ferrogarnet powder sample was ($0.50 \pm 0.01$ g). The resulting pellet was placed in an aluminum holder, pressed with a polyurethane foam sealant and secured with a lid.

Graphite electrodes used in AAES method were made of graphite rods with a diameter of 6 mm (AO Karbotek, Russian Federation), and ready-made electrodes of the “glass” shape (AO Karbotek, Russian Federation) were also applied. Graphite electrodes were prepared by means of a Krater-2M device (VMK-Optoelectronics, Russian Federation). The sample was diluted with graphite powder, pure in terms of target impurities (AO Karbotek, Russian Federation). High-purity sodium chloride (NaCl); sodium fluoride (NaF); elemental sulfur (S); potassium chloride (KCl); germanium oxide (GeO) were used as carriers. Reference samples to plot the calibration curve were made of high purity iron ($Fe_3O_4$), yttrium ($Y_2O_3$), gallium ($Ga_2O_3$), and cerium ($CeO_2$) oxides in a ratio of 2.5:2.5:2.5:1, which were then mixed with graphite powder with a known content of the impurities being determined.

High-purity nitric ($HNO_3$ – 70%) and hydrochloric (HCl – 35–38%) acids were used for sample preparation for ICP-MS and ICP-OES analysis. All dissolutions and dilutions were conducted by means of deionized water with a resistivity of 18.2 MΩ cm at 25°C. Aqueous calibration solutions for ICP-MS and ICP-OES were prepared from multi-element and single-element standard solutions (High-Purity Standards, USA) by serial dilution to different volumes with a 2 % $HNO_3$ mixture. The calibration dependence in ICP-MS method was constructed by means of multielement solutions with concentrations of the analytes being determined of 1–100 $\mu$g/L, and in the ICP-OES method of 0.1–100 mg/L for Mg,

TABLE 3. Instrumental operating conditions of the mass spectrometer

| | |
|---|---|
| Forward power, W | 1300 |
| Coolant gas flow, L·min$^{-1}$ | 15 |
| Auxiliary gas flow, L·min$^{-1}$ | 12 |
| Nebulizer gas flow, L·min$^{-1}$ | 0.95 |
| Sample flow rate, rpm | 30 |
| Sampling depth, relative units | 0 |
| Helium flow rate, mL·min$^{-1}$ | 6.5 |
| Level of oxide ions, % | $< 2$ |
| Level of doubly charged ions, % | $< 1.5$ |
| Measurement mode | Peak hopping |
| Pneumatic nebulizer | Meinhard, PerkinElmer |
| Spray chamber | Quartzconical, Peltiercooled |
| Isotopes of elements being determined, m/z | $^{24/25}$Mg, $^{27}$Al, $^{29}$Si, $^{42}$Ca, $^{45}$Sc, $^{52/53}$Cr, $^{55}$Mn, $^{59}$Co, $^{62}$Ni, $^{63}$Cu, $^{68}$Zn, $^{82}$Se, $^{111/112}$Cd, $^{117}$Sn, $^{125}$Te, $^{139}$La, $^{141}$Pr, $^{145/146}$Nd,$^{147/149}$Sm, $^{151}$Eu, $^{160}$Gd, $^{159}$Tb, $^{161/162}$Dy, $^{165}$Ho, $^{167/168}$Er, $^{169}$Tm, $^{172-174}$Yb, $^{175}$Lu, $^{207/208}$Pb |
| Internal standard | $^{103}$Rh, $^{115}$In |

Al, Si, Ca, Sc, Cr, Mn, Co, Ni, Cu, Zn, Se, Cd, Sn, Te, La, Pr, Nd, Sm, Eu, Gd, Tb, Dy, Ho, Er, Tm, Yb, Lu, Pb; and 10–500 mg/L for Fe, Ga, Y, Ce.

The decomposition of the samples was carried out using a MARS6 microwave autoclave system with microwave heating (CEM Corp., USA) and Easy-PrepiWave vessels (CEM Corp., USA). The dissolution was performed using previously established conditions, namely, using an acid mixture (5 ml $H_2O$, 2 ml $HNO_3$, 5 HCl) and a temperature-time program (hold time – 30 min, hold temperature – 220°C). The decomposition method was estimated for a sample weight of 0.1 g [35].

## 3. Results and discussion

### 3.1. Materials

According to the results of XRD, after synthesis and annealing in vacuum, the particle size of $Y_{3-x}Ce_xFe_{5-y}Ga_yO_{12}$ was ∼100 nm, the phase composition was homogeneous.

Fig. 1 shows a SEM-image of $Y_{2.5}Ce_{0.5}Fe_{2.4}Ga_{2.6}O_{12}$ powder. The powder is seen not to have any heterogeneous formations. The particles themselves are characterized by unimodality, and the crystallite growth faces are clearly expressed. The particle size is ∼100 nm.

### 3.2. X-ray fluorescence analysis

The studies into the XRF conditions of multicomponent materials, such as cerium-doped yttrium ferrogarnet, are aimed at increasing the selectivity of the signal of the elements being determined to achieve the required accuracy of the analysis results (RSD $\leq$ 10%). It is necessary to control the ratio and uniformity of the matrix and alloying element distribution in the sample, which are fundamental indicators in the development and production of garnets. It is particularly difficult to achieve the required accuracy indicators when using the FPM. Despite its advantage – the absence of standardization, it can be difficult to achieve the required metrological indicators, which needs a competent choice of analysis conditions.

The algorithm for studying and selecting the XRF conditions includes a number of operating parameters of the spectrometer (Fig. 2).

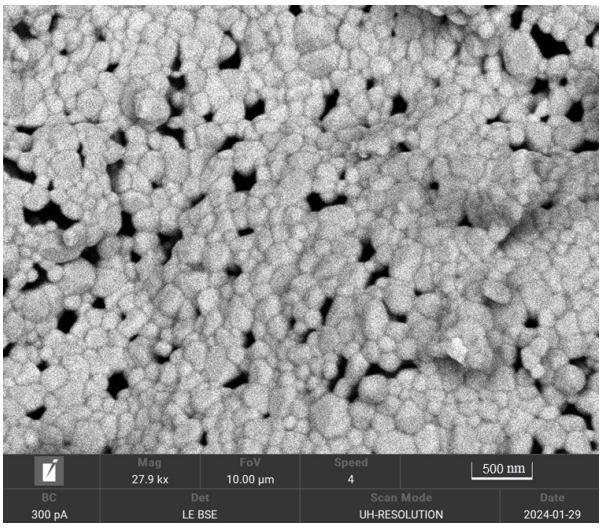


FIG. 1. SEM-image of the obtained particles of yttrium-iron garnet ($Y_{2.5}Ce_{0.5}Fe_{2.4}Ga_{2.6}O_{12}$)

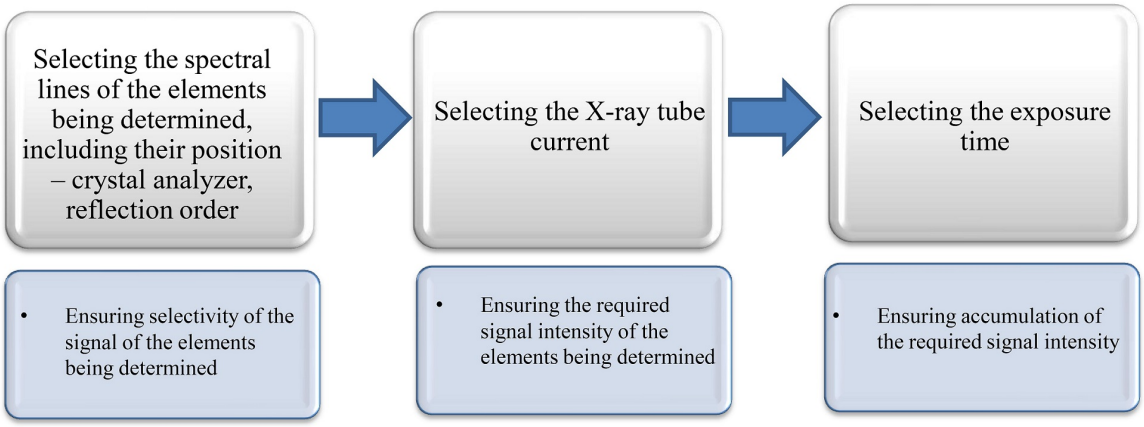


FIG. 2. Methodological approach to the selection of the XRF conditions

First, it is necessary to select the spectral lines of the elements being determined. While selecting analytical lines, one must focus on the absence of spectral interference from matrix and impurity elements on the signal of target analytes, as well as the ability to assess the noise level near the lines being studied. The SPECTROSCAN MAX-GVM spectrometer is equipped with four analyzer crystals (LiF200, PET, RbAP, C002) with different values of inter-planar distances, which allows optimizing the conditions to determine elements in different wavelength ranges and to establish the most optimal and overlap-free lines. Each analyzer crystal has 2 reflection orders.

To select the spectral lines of Fe, Ga, Y and Ce, the spectral line atlas embedded in the instrument software was used, with it taking into account the overlaps of all the elements being determined. Fig. 3 shows the spectrum of the $Y_{2.5}Ce_{0.5}Fe_{2.5}Ga_{2.5}O_{12}$ sample, recorded using the LiF200 crystal analyzer in the first reflection order. To determine the target elements, the lines recorded using this crystal analyzer were selected, since they are the least susceptible to mutual overlaps. The selected lines of elements being determined are presented in Table 1.

The criterion for selecting the X-ray tube current and exposure time is the fulfillment of the condition: [Signal intensity] $\times$ [Exposure time] $\leq$ 300.000 pulses. This rule is due to the detector capabilities, since too high current leads to its failure. The exposure time should be sufficient for signal accumulation, but not too long, in order to avoid unnecessary interference and reduce the analysis time. We were faced with the task of determining the main and alloying components; in order to prevent the detector overload and the spectrometer failure. While determining Fe, Ga, Y and Ce, the effect of the current near the lower limit of the range – from 0.1 to 3.5 mÅ and the exposure time – from 10 to 50 sec was studied. For Fe and Ga, the currents selected were 0.5 mÅ, for Y – 0.1 mÅ (such low currents are due to the high intensities of the selected spectral lines), and for Ce – 1.5 mÅ. The exposure time for all elements was 10 sec (Table 1).

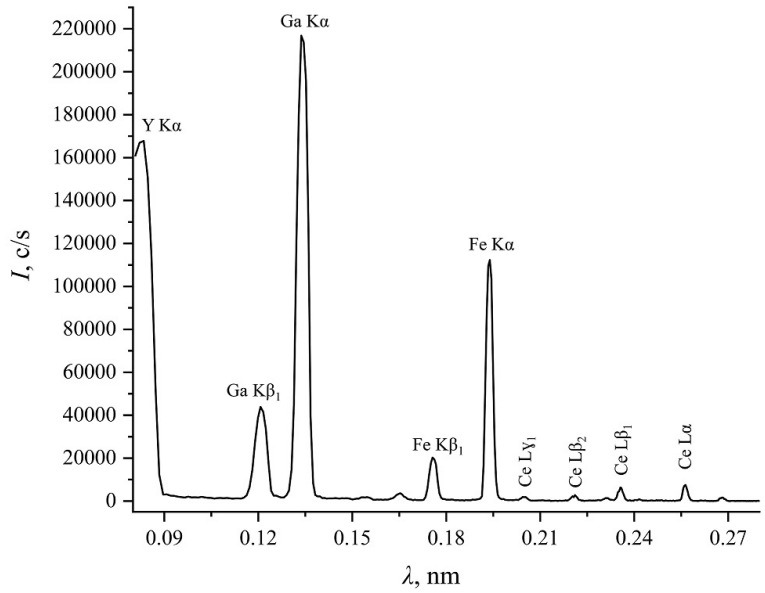


FIG. 3. XRF spectrum of $Y_{2.5}Ce_{0.5}Fe_{2.5}Ga_{2.5}O_{12}$ sample

### 3.3. Arc atomic emission analysis

The study of arc atomic emission analysis (AAEA) conditions is aimed at ensuring selectivity, intensity (I) and stability of the signal of the elements to be determined. In the light of this, a number of analysis conditions were studied to develop AAES to determine target impurities in cerium-doped yttrium ferrogarnets (Fig. 4).

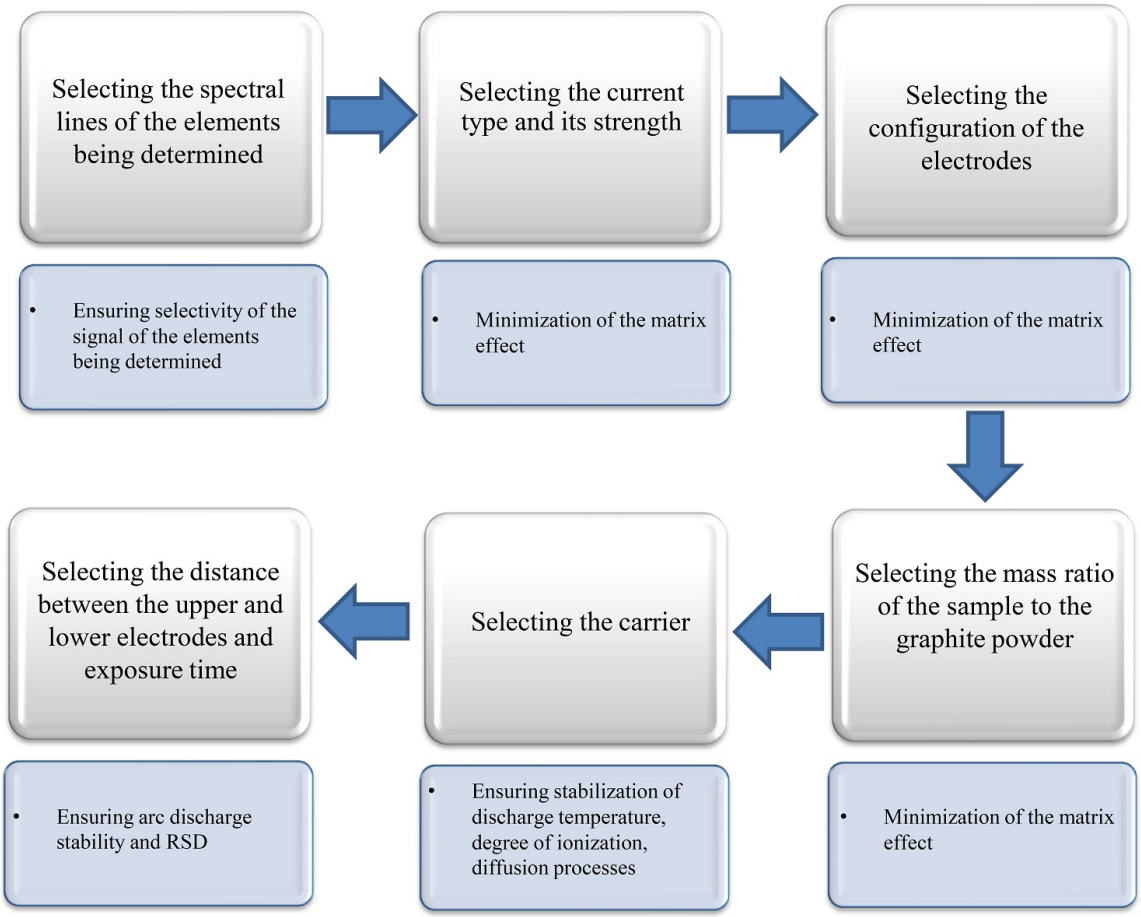


FIG. 4. Methodological approach to the selection of conditions for AAEA

Selecting the analytical lines of the elements being determined is based on the sample composition. Analytical lines are usually selected from the most sensitive lines of the spectrum; these include lines with the lowest excitation potential values. A large number of sensitive lines of rare earth elements are located in the range of 250–350 nm. The most sensitive lines of rare earth elements are in the range of 300–450 nm. The atlas of spectral lines and the signal/noise ratio were used to select the lines. In cases where it was not possible to select a line free of spectral overlaps, the contribution of spectral interference to the signal intensity of the analyte being determined was taken into account using software. The selected analytical lines are presented in Table 2.

One of the most important factors influencing the processes of evaporation, atomization and excitation of elements is the current type and its strength. The current shape, its polarity and intensity have a direct effect on the evaporation of the analytes being determined and the resulting spectrum. Given this, the behavior of the impurities being determined was studied under conditions of direct, alternating and intermittent current. In addition, the current strength was varied from 5 to 20Å. The best result was obtained with a direct positive current of 15Å.

The shape and size of graphite electrodes affect the flow of the sample into the arc plasma. The configuration of the electrode used allows one to set the temperature in the arc cloud and, accordingly, the evaporation rate of impurities. REE are slowly evaporating substances. In the volatility series, they are located at the end of the series together with low-volatile metals. Therefore it is reasonable to use electrodes with a narrow constriction below the bottom of the recess (configuration of the lower graphite electrode is “glass”) with thin walls (up to 1 mm) (Fig. 5).

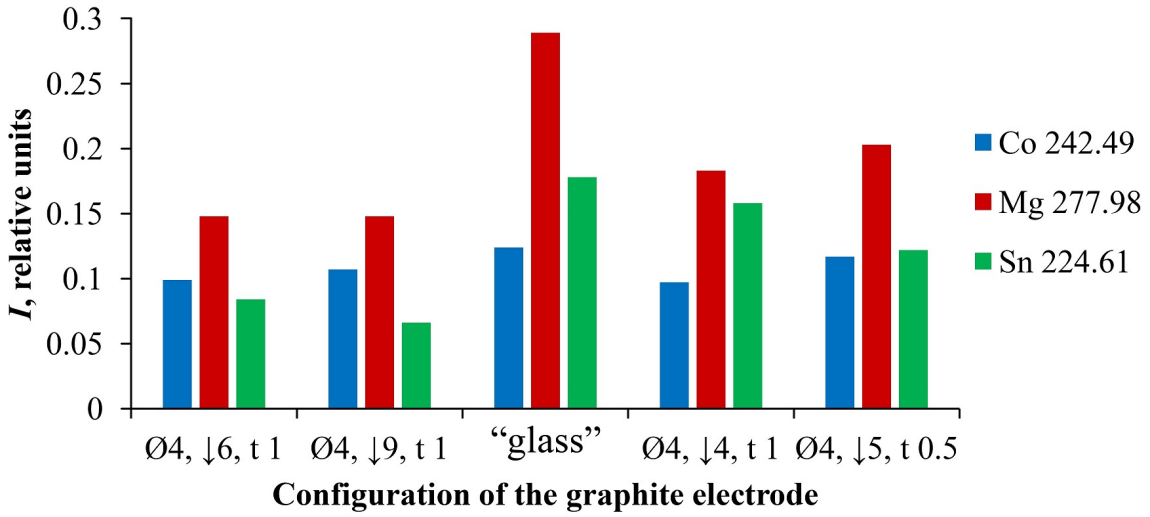


FIG. 5. Selection of an electrode for the determination of target impurities in nanosized yttrium-iron-gallium garnets (↓ — crater depth, mm; Ø — diameter, mm; t — crater wall thickness, mm)

The configuration of the upper graphite electrode of a cone 60° was chosen, since the discharge is more stable and is evenly distributed over the entire working surface of the electrode during the arc burning process.

To ensure robust conditions to determine target impurities, the analyzed sample was mixed with graphite powder (g.p.) in a certain ratio. This minimized the matrix effect. However, if the dilution is too great, the signal intensity of the analytes decreases. Therefore, it is necessary to select the optimal mass ratio of the sample to the g.p. Studies on selecting the mass ratio of the sample to the g.p. showed that the most optimal ratio is 5:1.

To stabilize the discharge temperature, the degree of elements ionization and diffusion processes in a direct or alternating current arc, special chemically active additives (carriers) – were introduced into the sample. Their introduction into the arc cloud led to an increase in the conductivity of the arc plasma column, caused a decrease in the voltage between the electrodes and a decrease in the voltage gradient in the arc plasma column, which in turn led to a decrease in the temperature in the plasma and an increase in the electron concentration [36,37]. All these processes resulted in an increase in the intensities of the lines being determined and an increase in the sensitivity of the method. In this work, NaCl showed the best result as a carrier for target impurities.

The distance between the upper and lower electrodes (inter-electrode distance) can be varied to achieve the most stable sample burnout. The greater the inter-electrode distance, the higher the voltage on it, which helps to reduce the signal intensity of the analytes. This leads to the fact that the limits of detection and determination (LOD) of target elements increase. Reducing the length of the inter-electrode distance helps to spatially stabilize the discharge. It is important that the distance remains constant, otherwise the repeatability standard deviation (RSD) of the analysis results increases. An inter-electrode distance of 3 mm was chosen for all materials, since it was the most appropriate from the viewpoint of the stability of the plasma discharge during the arcing.

To control the exposure time, it is necessary to study the evaporation curves in detail. Since different elements evaporate at different rates, it is necessary to set the exposure time during which all impurities will completely evaporate. If the time is too long, a noise signal will accumulate; if it is too short, the sample or impurities in it will not have time to completely ionize. Given the chance, it is better to set an individual determination time for each element due to its different volatility. It was established that 60 sec is sufficient to determine all target impurities (Fig. 6).

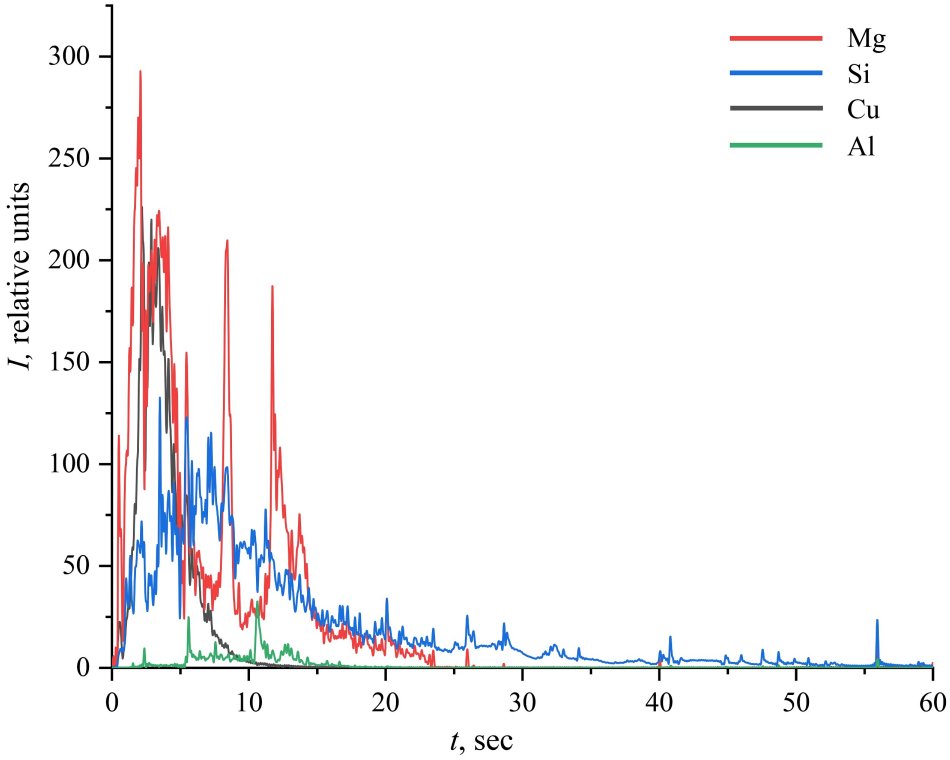


FIG. 6. Evaporation curves of Mg, Si, Cu, Al

The conditions of AAEA selected during the study are presented in Table 2. The use of these conditions (Table 2) provides the LOD of target impurity elements at the level of $3.0{\cdot}10^{-6}$–$6.0{\cdot}10^{-4}$ wt. %.

### 3.4. Inductively coupled plasma mass spectrometry analysis

The study of the ICP-MS conditions is aimed at minimizing the matrix effect, ensuring selectivity and signal intensity of target analytes. A number of analysis conditions were accordingly studied to develop ICP-MS to determine target impurities in cerium-doped yttrium ferrogarnets (Fig. 7).

Selecting the isotopes of the elements being determined in ICP-MS is justified by the complex composition of cerium-substituted yttrium iron garnets. The presence of several matrix elements (Fe, Ga, Y, Ce) leads to the formation of a large number of polyatomic ($^{n}M^{1}H^{+}$, $^{n}M^{12/13}C^{+}$, $^{n}M^{14/15}N^{+}$, $^{n}M^{16}O^{+}$, $^{n}M^{16}O^{1}H^{+}$) and doubly charged ($^{n}M^{++}$) ions. The formation of these ions in plasma causes an increase in the signal intensity of a number of target analytes and, accordingly, to an increase in their LOD (Table 4).

The greatest influence on the LOD was exerted by oxide and hydroxide ions ($^{n}Ce^{16}O^{+}$, $^{n}Ce^{16}O^{1}H^{+}$) formed from Ce (Table 4). This resulted in a significant increase in the apparent concentration for elements such as Gd and Tb, which was a prerequisite for studying the effect of the He consumption rate in the collision cell in their determination. The isotopes of the target analytes selected for analysis are given in Table 3.

The matrix effect was expressed as the suppression of the signal intensity of the elements being determined with increasing concentration of the matrix element [33]. Several complementary approaches were used to minimize the matrix effect: dilution of the analyzed solutions, introduction of an internal standard, selection of the operating parameters of the spectrometer (nebulizer gas flow, voltage on the extractor lens, provided that it is present in the optical system of the spectrometer) [29]. The nebulizer gas flow in the study varied in the range of 0.6–1.2 L·min$^{-1}$. The minimum matrix effect and maximum analytical signals for most elements were obtained at nebulizer gas flow of 0.95 L·min$^{-1}$. The level of doubly charged ions did not exceed 2.0 %. Fig. 8 shows the dependence of the signal intensity of the elements characterizing the mass scale ($^{25}$Mg, $^{65}$Cu, $^{137}$Ba, $^{232}$Th) on the concentration of the main elements simulating the composition of the material ($Y_{2.5}Ce_{0.5}Fe_{2.5}Ga_{2.5}O_{12}$). The magnitude of the matrix effect was estimated as $I_i/I_0$, where $I_i$ is the signal intensity of the analyte isotope in a solution with the main elements (0–500 $\mu$g/ml matrix), $I_0$ is the signal

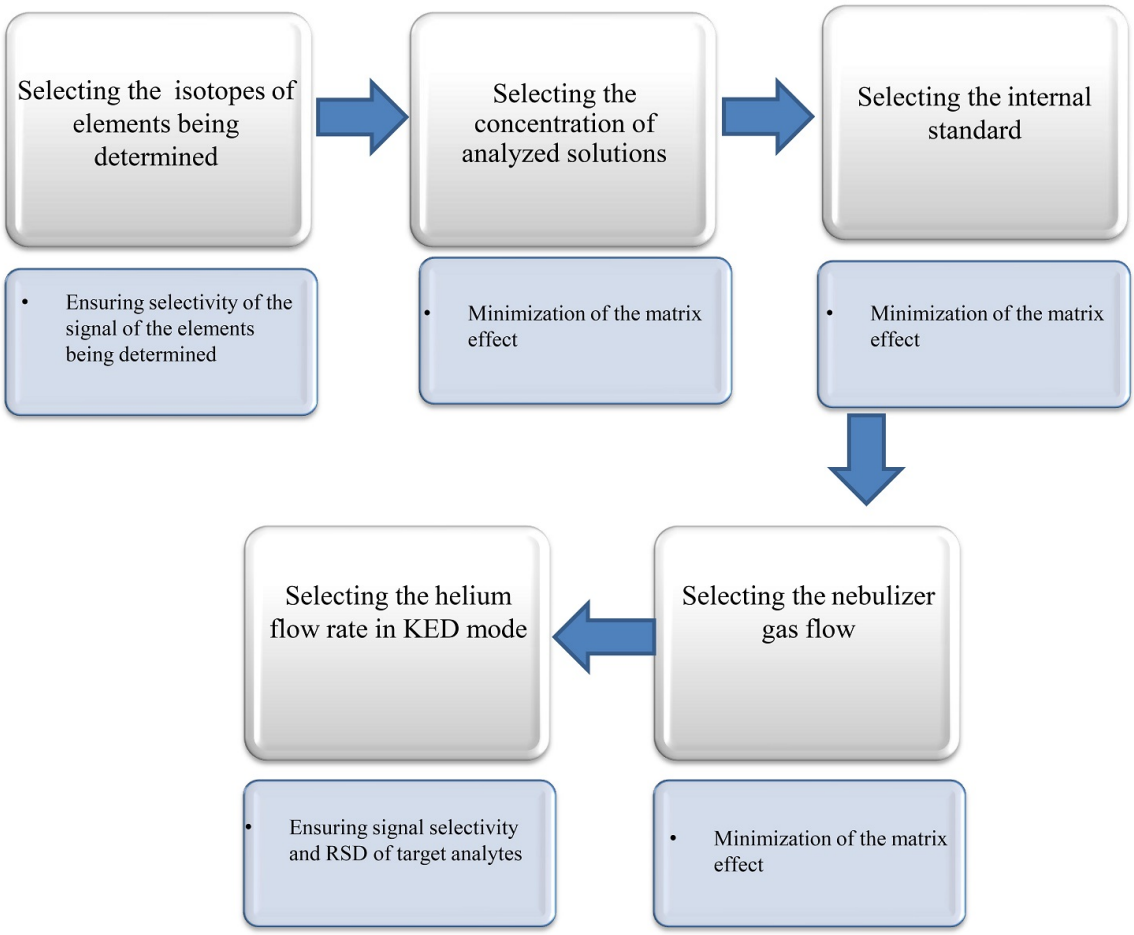


FIG. 7. Methodological approach to the selection of conditions for ICP-MS analysis

intensity of the element being determined in a pure nitric acid solution. $^{103}$Rh and $^{115}$In were used as internal standards to reduce the matrix effect (Fig. 8).

As can be seen in Fig. 8, both the introduction of two elements as an internal standard and a nebulizer gas flow of 0.95 L·min$^{-1}$ lead to a noticeable reduction in the matrix effect, which allows for the analysis of more concentrated solutions (up to 500 mg/l).

One of the most common techniques to reduce the influence of polyatomic ions on the LOD of analytes is the use of a collision cell with an inert gas – He (KED mode). With that in mind, the effect of helium flow rate on the apparent concentration of $^{n}Ce^{16}O^{+}$, $^{n}Ce^{16}O^{1}H^{+}$ ions was studied in determining of Gd and Tb in the KED mode. The studied solutions contained 500 mg/L of the main elements simulating the composition of $Y_{2.5}Ce_{0.5}Fe_{2.5}Ga_{2.5}O_{12}$. With an increase in a helium flow rate, the apparent concentration of $^{n}Ce^{16}O^{+}$, $^{n}Ce^{16}O^{1}H^{+}$ ions was expected to decrease (Table 5).

The results showed that the optimal helium flow rate is 6.5 mL·min$^{-1}$. While using this helium flow rate, an order-of-magnitude decrease in the apparent concentration of $^{n}Ce^{16}O^{+}$, $^{n}Ce^{16}O^{1}H^{+}$ ions was achieved.

The conditions of ICP-MS analysis selected during the study (Table 3) provide the LOD of target impurity elements at the level of $1{\cdot}10^{-6}$–$2.5{\cdot}10^{-3}$ wt. %.

### 3.5. The accuracy of the obtained results

The accuracy of the obtained results was confirmed using the added-found method and analysis of a sample by ICP-OES method using a previously developed technique [35]. For the added-found method, solutions containing 1.0, 10.0, and 50.0 $\mu$g/L of target impurity elements (Mg, Al, Si, Ca, Sc, Cr, Mn, Co, Ni, Cu, Zn, Se, Cd, Sn, Te, La, Pr, Nd, Sm, Eu, Gd, Tb, Dy, Ho, Er, Tm, Yb, Lu, Pb). The repeatability standard deviation for the target analytes in ICP-MS was 1–5 relative %, in DAES was 3–10 relative %, in XRF was 7–10 relative %.

The use of AAES and ICP-MS ensures control of the impurity composition of yttrium iron garnets in the ranges from $1{\cdot}10^{-6}$ to 1 wt. %. ICP-MS method has lower LOD for the determination of Sc ($2{\cdot}10^{-6}$ wt. %), Cr ($6{\cdot}10^{-6}$ wt. %), Ni ($8{\cdot}10^{-6}$ wt. %), Cu ($6{\cdot}10^{-6}$ wt. %), Zn ($6{\cdot}10^{-6}$ wt. %), Cd ($2{\cdot}10^{-6}$ wt. %), Te ($2{\cdot}10^{-6}$ wt. %), La ($2{\cdot}10^{-6}$ wt. %), Nd ($2{\cdot}10^{-6}$ wt. %), Sm ($2{\cdot}10^{-6}$ wt. %), Eu ($3{\cdot}10^{-6}$ wt. %), Ho ($2{\cdot}10^{-6}$ wt. %), Tm ($2{\cdot}10^{-6}$ wt. %), Yb ($1{\cdot}10^{-6}$ wt. %), Lu

TABLE 4. Polyatomic ions that interfere with the determination of target analytes in a solution containing 500 mg/L of main elements simulating the composition $Y_{2.5}Ce_{0.5}Fe_{2.5}Ga_{2.5}O_{12}$

| Element | Isotop | Polyatomic Ion | Apparent Concentration of the Element, $\mu$g/L |
|---|---|---|---|
| Mn | $^{55}$Mn | $^{54}Fe^{1}H^{+}$ | 0.30 |
| Co | $^{59}$Co | $^{58}Fe^{1}H^{+}$ | 0.48 |
| Zn | $^{66}$Zn | $^{54}Fe^{12}C^{+}$ | 0.10 |
| Pr | $^{141}$Pr | $^{140}Ce^{1}H^{+}$ | 1.20 |
| Nd | $^{143}$Nd | $^{142}Ce^{1}H^{+}$ | 0.85 |
| Sm | $^{149}$Sm | $^{136}Ce^{13}C^{+}$ | 0.04 |
| | $^{152}$Sm | $^{136}Ce^{16}O^{+}$, $^{138}Ce^{14}N^{+}$, $^{140}Ce^{12}C^{+}$ | 36.5 |
| | $^{154}$Sm | $^{138}Ce^{16}O^{+}$, $^{140}Ce^{14}N^{+}$, $^{142}Ce^{12}C^{+}$ | 57.0 |
| Eu | $^{151}$Eu | $^{136}Ce^{15}N^{+}$ | 0.001 |
| | $^{153}$Eu | $^{136}Ce^{16}O^{1}H^{+}$, $^{138}Ce^{13}C^{+}$, $^{138}Ce^{15}N^{+}$, $^{140}Ce^{13}C^{+}$ | 1.5 |
| Gd | $^{155}$Gd | $^{138}Ce^{16}O^{1}H^{+}$, $^{140}Ce^{15}N^{+}$ | 0.60 |
| | $^{156}$Gd | $^{140}Ce^{16}O^{+}$, $^{142}Ce^{14}N^{+}$ | 3583 |
| | $^{157}$Gd | $^{140}Ce^{16}O^{1}H^{+}$, $^{142}Ce^{15}N^{+}$ | 1982 |
| | $^{158}$Gd | $^{142}Ce^{16}O^{+}$ | 468 |
| Tb | $^{159}$Tb | $^{142}Ce^{16}O^{1}H^{+}$ | 44.0 |

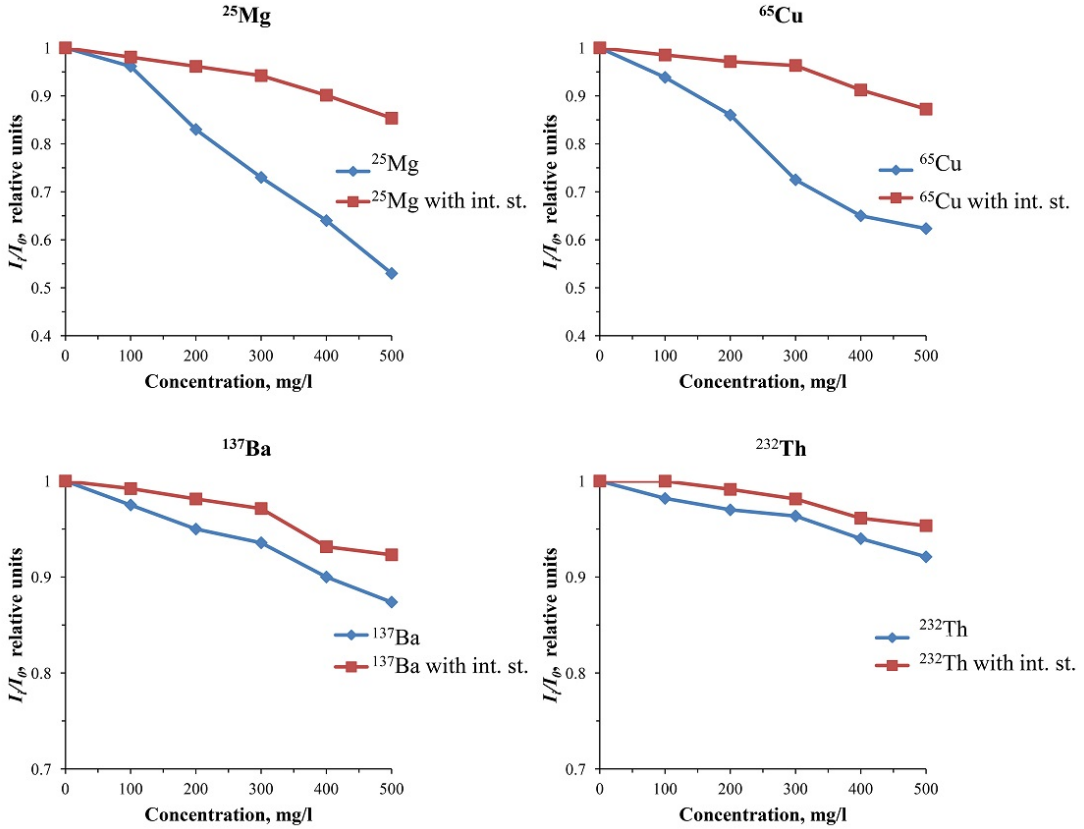


FIG. 8. Dependence of the signal intensity of the determined elements on the concentration of matrix elements in the solutio

TABLE 5. Apparent concentration of the elements being determined depending on a helium flow rate

| Isotop | Apparent Concentration of the Element, $\mu$g/L | | | |
|---|---|---|---|---|
| | He – 0 mL·min$^{-1}$ | He –5.0 mL·min$^{-1}$ | He –6.5 mL·min$^{-1}$ | He –7.25 mL· min$^{-1}$ |
| $^{155}$Gd | 0.60 | 0.08 | 0.01 | 0.003 |
| $^{159}$Tb | 44.0 | 0.62 | 0.02 | 0.01 |

($4{\cdot}10^{-6}$ wt. %). The use of AAES allowed one to reduce the LOD in determining of Si ($5{\cdot}10^{-4}$ wt. %), Mn ($3{\cdot}10^{-6}$ wt. %), Co ($2{\cdot}10^{-5}$ wt. %), Pr ($8{\cdot}10^{-5}$ wt. %), Tb ($9{\cdot}10^{-6}$ wt. %). AAES and ICP-MS have similar LOD for Mg ($2{\cdot}10^{-5}$ wt. %), Al ($2{\cdot}10^{-5}$ wt. %), Ca ($1{\cdot}10^{-4}$ wt. %), Se ($4{\cdot}10^{-4}$ wt. %), Sn ($1{\cdot}10^{-5}$ wt. %), Gd ($1{\cdot}10^{-5}$ wt. %), Dy ($1{\cdot}10^{-6}$ wt. %), Er ($2{\cdot}10^{-6}$ wt. %), Pb ($2{\cdot}10^{-6}$ wt. %). The joint use of the studied spectral methods ensures high accuracy and reliability of the results and allows for the expansion of the range of target analytes and the boundaries of the contents being determined.

## 4. Conclusions

The conditions of XRF, AAES and ICP-MS analysis of synthesized nanocrystalline cerium-substituted yttrium-iron-gallium garnets of the composition $Y_{3-x}Ce_xFe_{5-y}Ga_yO_{12}$ (where $x$ = 0.4–0.5, and $y$ = 2.4–2.6) were studied. Due to the optimization of the conditions of XRF, AAES and ICP-MS analysis, it was possible to improve the analytical characteristics in determining the target elements of the materials. In particular, the selected operating parameters of XRF (exposure time – 10 sec, tube current – 0.5–1.5 mÅ) enabled to achieve RSD less than 10 relative %. By the AAES determination of target impurity elements, the use of a "glass" shaped electrode, NaCl as a carrier, current strength of 15 Å, inter-electrode distance of 3 mm and a mass ratio of the sample to the graphite powder of 5:1 provided the best intensity and stability of the analyte signal, which allowed one to reduce the LOD to $3.0{\cdot}10^{-6}$–$6.0{\cdot}10^{-4}$ wt. % and RSD no more than 10 relative %. When determining Gd and Tb by ICP-MS, the use of helium flow rate of 6.5 mL·min$^{-1}$ in the KED mode enabled to reduce the LOD for these elements by an order of magnitude. The use of two internal standards ($^{103}$Rh, $^{115}$In) and nebulizer gas flow of 0.95 L·min$^{-1}$ allowed for a minimal matrix effect when analyzing solutions with a concentration of up to 500 mg/l of the base, which ensured the LOD of $1{\cdot}10^{-6}$–$2.5{\cdot}10^{-3}$ wt. % and RSD 1–5 relative %. The combined use of AAES and ICP-MS methods ensured the LOD for target impurity elements at the level of n·$10^{-6}$–n·$10^{-4}$ wt. %.

## References


[1] Dehghani D.O., Shokrollahi H., Yang H. The enhancement of the Ce-solubility limit and saturation magnetization in the $Ce_{0.25}Bi_xPr_yY_{2.75-x-y}Fe_5O_{12}$ garnet synthesized by the conventional ceramic method. *Ceramics International*, 2020, **46**(3), P. 2709–2723.

[2] Shen T., Dai H., Song M., Liu H., Wei X. Structure and Magnetic Properties of Ce-Substituted Yttrium Iron Garnet Prepared by Conventional Sintering Techniques. *Journal of Superconductivity and Novel Magnetism*, 2017, **30**, P. 937–941.

[3] Jung H.K., Kim C.H., Hong A.-R., Lee S.H., Kim T.C., Jang H.S., Kim D.H. Luminescent and magnetic properties of cerium-doped yttrium aluminum garnet and yttrium iron garnet composites. *Ceramics International* 2019, **45**, P. 9846–9851.

[4] Hapishah A.N., Hamidon M.N., Syazwan M.M., Shafiee F.N. Effect of grain size on microstructural and magnetic properties of holmium substituted yttrium iron garnets ($Y_{1.5}Ho_{1.5}Fe_5O_{12}$), *Results in Physics*, 2019, **14**, P. 102391.

[5] Gota T., Onbasli M.C., Kim D.H., Singh V., Inoue M., Kimerling L.C., Ross C.A. A nonreciprocal racetrack resonator based on vacuum-annealed magnetooptical cerium-substituted yttrium iron garnet. *Optics Express*, 2014, **22**, P. 19047–19054.

[6] Randoshkin V.V., Chervonenkis A.Ya. *Applied magneto-optics*, Moscow, Energoatomizdat, 1990, 320 p.

[7] Smirnova M.N., Glazkova I.S., Nikiforova G.E., Kop'eva M.A., Eliseev A.A., Gorbachev E.A., Ketsko V.A. Synthesis of Ce:YIG nanopowder by gel combustion. *Nanosystems: Physics, Chemistry, Mathematics*, 2021, **12**(2), P. 210–217.

[8] Sharm V., Kuanr B.K. Magnetic and crystallographic properties of rare-earth substituted yttrium-iron garnet. *Journal of Alloys and Compounds*, 2018, **748**, P. 591–600.

[9] Bokshyts Y.V., Kichanov S.E., Shevchenko G.P., Tratsiak E.V., Parshikova E.A., Kozlenko D.P. Structure and luminescence properties of $(Y_{1-x}La_x)_3(La_{1-y}Ga_y)O_{12}$:$Ce^{+3}$. *Inorganic Materials*, 2019, **55**(8), P. 820–826.

[10] Smirnova M.N., Nikiforova G.E., Goeva L.V. One-stage synthesis of $(Y_{0,5}Bi_{0,5})_3(Fe_{0,5}Ga_{0,5})_5O_{12}$ garnet using the organometallic gel auto-combustion approach. *Ceramics international*, 2018, **45**(4), P. 4509–4513.

[11] Smirnova M.N., Nipan G.D., Nikiforova G.E. $(Y_{1-x}Bi_x)_3(Fe_{1-y}Ga_y)_5O_{12}$ Solid Solution Region in the Ieneke Diagram, *Inorganic materials*, 2018, **54**(7), P. 683–688.

[12] Shen T., Dai H., Song M. Structure and Magnetic Properties of Ce-Substituted Yttrium Iron Garnet Prepared by Conventional Sintering Techniques. *Journal of Superconductivity and Novel Magnetism*, 2017, **30**, P. 937–941.

[13] Lisnevskaya I.V., Bobrova I.A., Lupeiko T.G. $Y_3Fe_5O_{12}$/Na,Bi,Sr-doped PZT particulate magnetoelectric composites. *Journal of Magnetism and Magnetic Materials*, 2016, **397**, P. 86–95.

[14] Huang M., Zhang S. Growth and characterization of cerium-substituted yttrium iron garnet single crystals for magneto-optical applications *Applied Physics A*, 2002, **74**, P. 177–180.

[15] Teterina Yu.A., Smirnova M.N., Maslakov K.I., Teterin A.Yu., Kop'eva M.A., Nikiforova G.E., Ketsko V.A. Ionic and Phase Compositions of $Y_{2.5}Ce_{0.5}Fe_{2.5}Ga_{2.5}O_{12}$. Ferrogarnet Powder Produced by Gel Combustion. *Doklady Physical Chemistry*, 2022, **503**2, P. 45–49.

[16] Yushchuk S.I., Yuryev S.O., Moklyak V.V. Monocrystalline ferrogarnet films with low magnetizations and small magnetic losses. *Materials Today: Proceedings*, 2022, **62**, P. 5771–5774.
[17] Khivintsev Y.V., Sakharov V.K., Kozhevnikov A.V., Dudko G.M., Filimonov Y.A., Khitun A. Spin waves in YIG based magnonic networks: Design and technological aspects. *Journal of Magnetism and Magnetic Materials*, 2022, **545**, P. 168754.
[18] Jin L., Jia K., He Y., Wang G., Zhong Z., Zhang H. Pulsed laser deposition grown yttrium-iron-garnet thin films: Effect of composition and iron ion valences on microstructure and magnetic properties. *Applied Surface Science*, 2019, **483**, P. 947–952.
[19] Rao Y., Zhang D., Zhang H., Jin L., Yang Q., Zhong Z., Li M., Hong C., Ma B.O. Thickness dependence of magnetic properties in submicron yttrium iron garnet films. *Journal Physics D: Applied Physics*, 2018, **51**(43), P. 435001.
[20] Arkhipenko A.A., Koshel E.S., Baranovskaya V.B. Analysis of cerium oxide by arc atomic emission spectrometry. *Zavodskaya laboratoriya. Diagnostika materialov*, 2021, **87**(11), P. 19–25.
[21] Koshel E.S., Arkhipenko A.A., Baranovskaya V.B.. Lutetium oxide analysis by direct arc atomic emission spectrometry. *Analytics and control*, 2021, **25**(2), P. 70–83.
[22] Vasilyeva I.E. Shabanova E.V. Stages of arc atomic emission spectrometry development as applied to the solid geological samples' analysis. *Analytics and Control*, 2021, **25**(4), P. 280–295.
[23] Schramm R. Use of X-ray Fluorescence Analysis for the Determination of Rare Earth Elements. *Physical Sciences Reviews*, 2016, **1**(1), P. 20160061.
[24] Sitko R., Zawisza B., Czaja M. Fundamental parameters method for determination of rare earth elements in apatites by wavelength-dispersive X-ray fluorescence spectrometry. *Journal of Analytical Atomic Spectrometry*, 2005, **20**, P. 741–745.
[25] Bondarenko A.V., Belonovsky A.V., Katsman Ya.M. Application of the method of fundamental parameters in X-ray fluorescence analysis of pulp products of ore enrichment. *Mining Industry*, 2021, **5-2**, P. 84–88
[26] Beckhoff B., Kanngießer B., Langhoff N., Wedell R., Wolff H. H*andbook of Practical X-ray Fluorescence Analysis*; Part 5 Quantitative Analysis, Berlin/Heidelberg, Springer, 2006, 863 p.
[27] Karandashev V.K., Orlova T.V., Zybinsky A.M., Kordyukov S.V., Simakov V.A., Kolotov V.P. Analysis of niobium-rare-earth ores by inductively coupled plasma mass spectrometry. *Journal of Analytical Chemistry*, 2018, **7**, P. 364–373.
[28] Salem D.B., Barrat J.A. Determination of rare earth elements in gadolinium-based contrast agents by ICP-MS. *Talanta*, 2021, **221**, P. 121589.
[29] Korotkova N.A., Baranovskaya V.B., Petrova K.V. Microwave Digestion and ICP-MS Determination of Major and Trace Elements in Waste Sm-Co Magnets. *Metals*, 2022, **12**(8), P. 1308.
[30] eiga M., Mattiazzi P., S. de Gois J., Nascimentod P.C., Borgese D.L.G., Bohrer D. Presence of other rare earth metals in gadolinium-based contrast agents. *Talanta*, 2020, **216**, P. 120940.
[31] Tanner S.D., Baranov V.I., Bandura D.R. Reaction cells and collision cells for ICP-MS: a tutorial review. *Spectrochimica Acta Part B*, 2002, **57**, P. 1361–1452.
[32] Balaram V. Strategies to overcome interferences in elemental and isotopic geochemical analysis by quadrupole inductively coupled plasma mass spectrometry: A critical evaluation of the recent developments. *Rapid Commun Mass Spectrom*, 2021, **35**, P. e9065.
[33] Agatemor C., Beauchemin D. Matrix effects in inductively coupled plasma mass spectrometry: A review. *Analytica Chimica Acta*, 2011, **706**(1), P. 66–83.
[34] Makonnen Y., Beauchemin D. Investigation of a measure of robustness in inductively coupled plasma mass spectrometry. *Spectrochimica Acta Part B*, 2015, **103–104**, P. 57–62.
[35] Korotkova N.A, Petrova K.V., Baranovskaya V.B. Analysis of cerium-substituted yttrium iron garnet by inductively coupled plasma atomic emission spectrometry with preliminary microwave decomposition. *Zavodskaya laboratoriya. Diagnostika materialov*, 2023, **89**(11), P. 24–33.
[36] Rusanov A.K. *Fundamentals of quantitative spectral analysis of ores and minerals*, M., Nedra, 1971, 360 p.
[37] Baranovskaya V.B., Koshel E. *Arc atomic emission analysis of rare earth metals and their oxides*, M., Technosfera, 132 p.

*Submitted 20 November 2024; accepted 25 November 2024*

*Information about the authors:*

*Natalia A. Korotkova* – Kurnakov Institute of General and Inorganic Chemistry of the Russian Academy of Sciences, Leninskii prosp., 31, Moscow, 119991, Russia; ORCID 0000-0003-1269-6570; natalya.korotkova.95@mail.ru

*Alexandra A. Arkhipenko* – Kurnakov Institute of General and Inorganic Chemistry of the Russian Academy of Sciences, Leninskii prosp., 31, Moscow, 119991, Russia; ORCID 0000-0002-2242-8572; alexandra622@mail.ru

*Maria N. Smirnova* – Kurnakov Institute of General and Inorganic Chemistry of the Russian Academy of Sciences, Leninskii prosp., 31, Moscow, 119991, Russia; ORCID 0000-0003-2707-7975; smirnovamn@igic.ras.ru

*Vasilisa B. Baranovskaya* – Kurnakov Institute of General and Inorganic Chemistry of the Russian Academy of Sciences, Leninskii prosp., 31, Moscow, 119991, Russia; ORCID 0000-0002-0076-9990; baranovskaya@list.ru

*Marina S. Doronina* – Kurnakov Institute of General and Inorganic Chemistry of the Russian Academy of Sciences, Leninskii prosp., 31, Moscow, 119991, Russia; ORCID 0000-0003-4553-1019; ms.semenova@gmail.com

*Valerii A. Ketsko* – Kurnakov Institute of General and Inorganic Chemistry of the Russian Academy of Sciences, Leninskii prosp., 31, Moscow, 119991, Russia; ORCID 0000-0002-2075-1755; ketsko@igic.ras.ru

*Galina E. Marina* – Kurnakov Institute of General and Inorganic Chemistry of the Russian Academy of Sciences, Leninskii prosp., 31, Moscow, 119991, Russia; ORCID 0009-0000-2872-2150; gelim@mail.ru

*Conflict of interest*: the authors declare no conflict of interest.